EEET ECOLOGICAL ENGINEERING & ENVIRONMENTAL TECHNOLOGY

Ecological Engineering & Environmental Technology, 2025, 26(9), 326–336
https://doi.org/10.12912/27197050/209737
ISSN 2719–7050, License CC-BY 4.0

Received: 2025.08.01
Accepted: 2025.08.20
Published: 2025.09.01

Linking annual land subsidence to built-up density across coastal tourism zones via Sentinel-1 differential interferometric synthetic aperture radar

Moh Saifulloh[1,2*], I Nyoman Sunarta[3], M. Baiquni[4], Ni Made Trigunasih[5], I Made Adikampana[3]

[1] Marine Science Program Faculty of Marine Science and Fisheries, Udayana University, Badung, Indonesia
[2] Spatial Data Infrastructure Development Centre, Udayana University, Denpasar, Indonesia
[3] Doctoral Program of Tourism Sciences, Faculty of Tourism, Udayana University, Denpasar, Indonesia
[4] Department of Development Geography, Faculty of Geography, Universitas Gadjah Mada (UGM), Yogyakarta, Indonesia
[5] Soil Sciences and Environment, Faculty of Agriculture, Udayana University, Denpasar, Indonesia
* Corresponding author's e-mail: m.saifulloh@unud.ac.id

ABSTRACT

Uncontrolled urban expansion has intensified land subsidence in many cities, including Bali's coastal tourism zone. To provide the first area-wide assessment for South Bali, we mapped spatiotemporal subsidence from 2014–2022 using Differential InSAR (DInSAR) on Sentinel-1 SLC data, derived built-up density from Sentinel-2, and tested their association. We find persistent subsidence with typical rates of −10 to −60 mm/yr, local extremes near −70 mm/yr, and a multi-year mean near −40 mm/yr. Hotspots cluster in Padang Sambian, Dauh Puri, Sanur, Pemogan, and Dalung; field inspections documented wall cracking, floor settlement, and road depressions consistent with these clusters. Notably, despite drawing global attention over the past decade for overtourism, the Canggu tourism area shows no detectable subsidence in our analysis. At the full-area scale, the subsidence–density relationship is very weak (year-by-year correlations near zero: $r \approx -0.11$ to $+0.008$; $R^2 \approx 0.0006$–0.012). Using decade-average statistics (~2014–2022) and a focused evaluation within zones exhibiting both high built-up density and elevated annual subsidence ($n \approx 10{,}000$ pixel samples), the association remains very weak ($r = 0.045$; $R^2 \approx 0.21\%$), although statistically significant ($p < 0.05$). Thus, while built-up density exerts a detectable effect, its contribution is minimal, implying that other drivers are more influential at city scale. We recommend using these results as screening evidence for risk-aware planning, prioritizing investigation and monitoring in identified hotspots, and integrating geology, soils, hydrology, groundwater levels, and refined InSAR processing to strengthen attribution and target mitigation. Unrevealed factors remain a key challenge for us and future researchers to determine the primary causes of land subsidence in this tourism zone and urban center.

Keywords: urban agglomeration, urban tourism, coastal land deformation, DInSAR; Sentinel-1 SAR, land subsidence, built-up density, LOS displacement.

INTRODUCTION

The Earth's surface is a dynamic object, and the forces acting on it influence its shape. One phenomenon resulting from this dynamic nature is land subsidence, which has occurred frequently in various regions, particularly in large cities (Hussain et al., 2022; Karimzadeh and Matsuoka, 2020). Land subsidence is caused by surface processes and human activities such as excessive groundwater extraction and land subsidence due to the load of infrastructure and buildings, as well as the geological and topographical conditions of the area (Abidin et al., 2013; Bai et al., 2022; Sarah et al., 2021). Utilizing synthetic aperture radar (SAR) imagery technology to identify areas

that are potentially experiencing subsidence as an effort to mitigate geological disasters and as an initial step in providing information for urban planning and regional development (Hakim et al., 2020; Ibrahim et al., 2024; Sahu and Rawat, 2023). One of the radar technology methods that is quite effective for mapping land subsidence areas is differential interferometric synthetic aperture radar (DInSAR), which has a high level of accuracy and can monitor large areas in a short time (Pawluszek-Filipiak and Borkowski, 2020; Sowter et al., 2016).

The method of processing and utilizing radar data in Indonesia is still in the assessment stage, but its use to provide fast visual information already exists due to the lack of cloud-free optical satellite data and the advantages of radar satellite data that can monitor the surface without weather interference and is available during the day and night (Darbaghshahi et al., 2022; Wang et al., 2019). Therefore, this study will use radar data, namely Sentinel-1 image data, which can be downloaded for free. Sentinel-1 imagery has several other advantages, namely, it has better temporal resolution, has a special mission to map land subsidence with high precision, and has a very wide coverage area (20–400 km) (Cian et al., 2019; Fajrin et al., 2021; Fernández-Torres et al., 2024; Rafiei et al., 2022; Rateb and Abotalib, 2020).

Land subsidence generally occurred in urban areas such as the capital city of Jakarta during the period 1982–2010 at a rate of around 1–15 cm/year (Abidin et al., 2011), and the latest research for the duration of 2017–2022 produced an average of -10.96 cm/year (Harintaka et al., 2024). Furthermore, in the tourism area of Bali, particularly in the southern coastal region, land deformation was recorded at rates between -8 mm and -19 mm, with a maximum speed of -5 mm/year during the period from 2015 to 2018 (Dwiputra et al., 2020).

However, until now there has been no updated information regarding land subsidence in tourism areas, especially in the agglomeration centers in Bali. In fact, the increase in built-up land has been growing from time to time (Bhayunagiri and Saifulloh, 2023; Diara et al., 2024; Sunarta et al., 2022; Sunarta and Saifulloh, 2022a). For example, in the 2013–2021 period, there was a land conversion of up to 20.23 km^2 (Andyana et al., 2023). This situation is due to the presence of tourist attractions that trigger the development of tourism facilities such as restaurants, hotels, and other developments. This phenomenon has resulted in the development of increasingly developed areas year after year. Previous study stated that the increase in built-up land has an impact on the decline in agricultural land in coastal areas (Sunarta and Saifulloh, 2022a).

Spatial data on land subsidence in Bali's tourism areas is important for establishing urban regulations and spatial planning, as well as controlling excessive development in tourism centers. This information is also crucial for local stakeholders to maintain urban green spaces and minimize the impact of flooding and seawater intrusions caused by this land subsidence phenomenon due to its location in coastal areas. Therefore, we propose a study aimed at analyzing land subsidence spatially and temporally in tourism areas based on the latest data. We then link this correlation to urban density using a simple correlation analysis, thus providing concrete information regarding the relationship between the two variables.

METHOD

Research site

The local government has classified the southern coastline area of Bali Province, Indonesia, as an urban tourism area, and researchers are studying the effects of land subsidence there. It administratively encompasses North, East, West, and South Denpasar as well as Kuta and North Kuta in Badung Regency. The growth of developed areas and the number of tourists visiting these regions indicate that tourism has developed rapidly. Figure 1 shows the geographic coordinates of the case study location, which is located at 115°10'00"E–115°13'00" E and 08°36'00"S–08°45'00"S. The biophysical characteristics indicate that the study area is flat (0–8%) and has an elevation of 0–50 meters above sea level. While this is going on, other studies in the same region have looked at how the footprint of the built-up area has grown. The built-up area increased from 117.79 km^2 to 120.41 km^2 between 2013 and 2021 (Andyana et al., 2023) and has implications for other environmental degradation such as increased greenhouse gas emissions (Sunarta and Saifulloh, 2022b), due to low urban carbon absorption (Sudarma et al., 2024). This persistent trend of urbanization highlights the need for comprehending the effects of land alteration on land subsidence in the region.

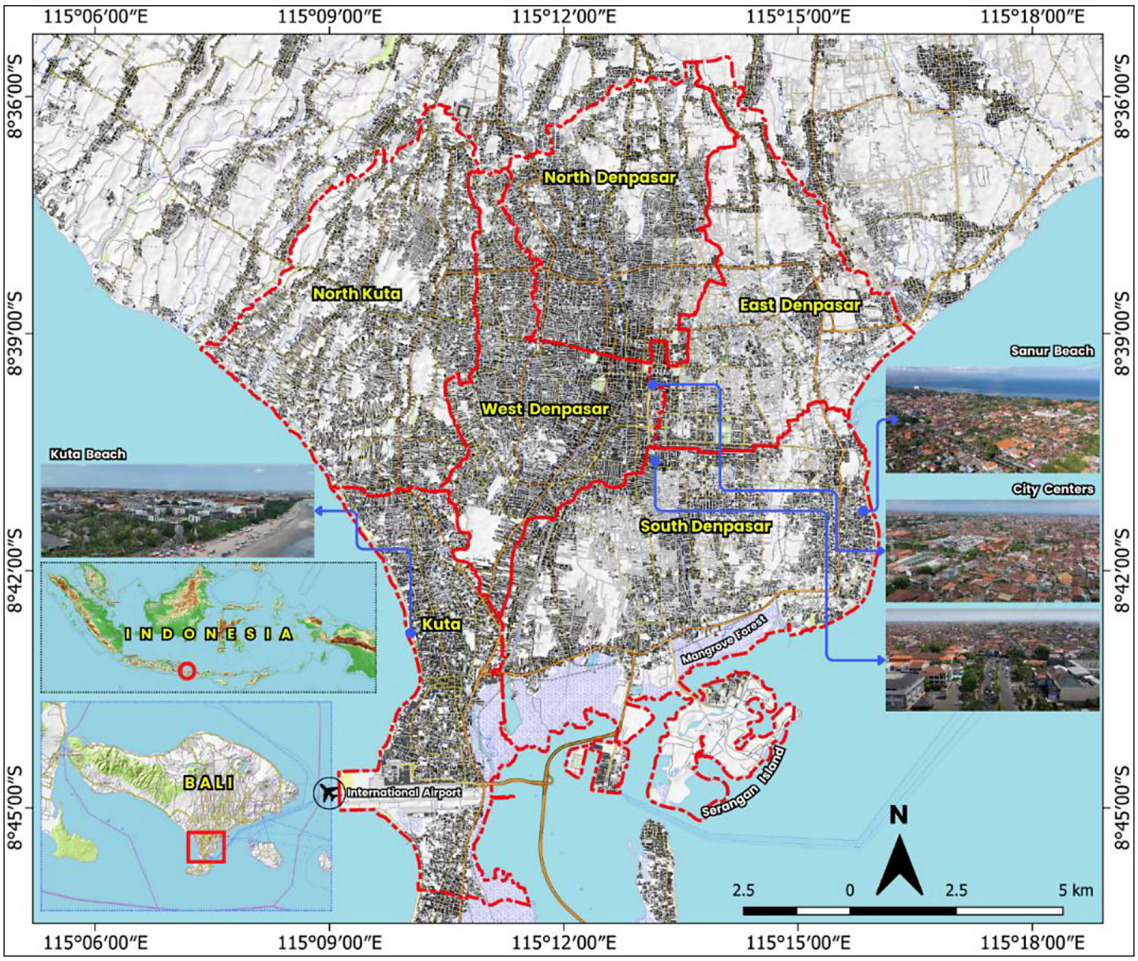

Figure 1. Case study area located in the coastal tourism hub and capital city of Bali Province, Indonesia. The red outline marks the administrative boundary of the study area, while the accompanying photograph highlights the densely built-up urban core of Denpasar and the adjacent industrial tourism zones along Sanur and Kuta Beaches

Sentinel-1 data processing

Primary remote sensing data for this investigation comes from Sentinel-1 radar imaging in Interferometric Wide Swath (IW) Level-1 SLC (single look complex) mode. Sentinel-1 consists of two satellites, Sentinel-1A and Sentinel-1B, that are in a constellation. They both follow the same orbital path, although their phases are opposite each other. This constellation is perfect for periodic investigation of ground surface deformation because each satellite has a 12-day repeat cycle, and data is acquired every 6 days overall (Islam et al., 2017). Developed as a component of the Copernicus Earth observation program, Sentinel-1 will provide worldwide data in areas like land management, climate change, oceans, disaster mitigation, and environmental security. This program was launched by the European Commission and the European Space Agency. In order to analyze ground subsidence, the DInSAR approach was used in conjunction with the GAMMA software on the ASF HyP3 platform. An interferometric pair was formed by selecting two Sentinel-1A images: one to serve as the reference image (the master) and the other as the secondary image (the slave). The first step of the processing is to co-register the two images by checking if their geometric and spatial baselines are congruent. The coherence values are used to validate the picture pair quality. These values quantify the phase correlation between the images, and a minimum threshold of 0.6 is used to verify the dependability of the results. After that, we'll use the minimum cost flow (MCF) technique to create an interferogram and begin the phase unwrapping procedure. Here, using Sentinel-1's radar wavelength (around 5.6 cm), we transform the phase values of the interferogram into the real distance disparities between the ground and the satellite. For every 2π phase change, there is a 2.8 cm shift in the LOS direction (Equation 1).

$$D_{LOS} = \frac{\lambda \cdot \phi}{4\pi} \quad (1)$$

where: D_{LOS} is the ground surface displacement value in meters, λ is the Sentinel-1 radar wavelength, and π is the unwrapping phase difference in radians. This is equal to the phase difference after unwrapping in radians, the value of the ground surface displacement in meters, and the wavelength of the Sentinel-1 radar.

Finding and mapping those negative values, which indicate regions with substantial land subsidence, is the primary goal of this study. The system-determined deformation reference points, namely the pixels with the highest coherence values at coordinates -8.66493°S and 115.21156°E, are likewise subjected to the correction process. A geometrically corrected and UTM Zone 50S-aligned GeoTIFF map showing line-of-sight displacement is the end result of this procedure. Elevation correction and field modeling are supported by 30-meter-resolution topographic data from the Copernicus GLO-30 DEM. The final product of the processing workflow is a map of the land's deformation, which may be used for spatial analysis to identify areas of significant subsidence and trends within the research area.

Built-up land density

This study utilizes both Sentinel-1 radar images and Sentinel-2 optical data to assess ground surface deformation and determine the normalized difference built-up index (NDBI). Coastal regions with high population densities may be more susceptible to land subsidence; this index can help pinpoint locations where man-made features like buildings and concrete infrastructure predominate. For spectral monitoring of land surfaces, the multi-channel optical satellite Sentinel-2 is invaluable, as it delivers data with a spatial resolution of 10–20 meters. Here is the formula that is used to calculate NDBI using the reflectance values from the SWIR and NIR channels (Zha et al., 2003) (Equation 2):

$$NDBI = \frac{(SWIR - NIR)}{(SWIR + NIR)} \quad (2)$$

where: *SWIR* refers to Band 11 (1610 nm) representing shortwave infrared, and *NIR* refers to Band 8 (842 nm) representing near-infrared in the Sentinel-2 imagery product.

This research makes use of Band 11 (1610 nm) for shortwave infrared and Band 8 (842 nm) for near-infrared. An area is more likely to be built up if its NDBI value is high; this value is created per pixel and interpreted geographically. In order to efficiently acquire and process multi-temporal image data, processing is carried out through Google Earth Engine (GEE) (Gorelick et al., 2017).

Analysing correlations

A statistical analysis was carried out using the Pearson correlation coefficient to ascertain the strength of the association between land subsidence and building density in the studied area. We opted for this approach because it quantifies the linear relationship between two continuous variables the Line-of-Sight (LOS) displacement value from Sentinel-1 data and the NDBI value from Sentinel-2 imaging and can tell us which way the relationship is going.

Both raster data sets must be extracted, and their coordinate systems and resolutions must be aligned before the analysis can begin. In order to remove inaccurate values (such as those caused by water bodies or dense vegetation), all overlapping pixels in the research region are removed using zonation and masking techniques. This process yields two sets of numerical data that can be compared statistically (Equation 3).

$$r = \frac{n\sum(xy) - \sum x \sum y}{\sqrt{[n\sum x^2 - (\sum x)^2] \cdot [n\sum y^2 - (\sum y)^2]}} \quad (3)$$

where: r is the Pearson correlation coefficient, r is the NDBI variable (built-up density), r is the LOS displacement variable (land subsidence), n is the number of data pairs.

Identify the number of data pairs, the Pearson correlation coefficient, the NDBI variable (built-up density), and the LOS displacement variable (land subsidence). A value between -1 and +1 is possible for the coefficient. The tendency for uplift (land subsidence reduces) increases as the NDBI value increases (near to +1 indicates a strong positive association). On the flip side, a number around -1 suggests a significant negative correlation, which means that land subsidence or the negative displacement value increases in response to the built-up density. A number approaching zero suggests that the two variables are not significantly related in a linear fashion.

RESULTS

Land subsidence (2014–2022)

We analyzed Sentinel-1 C-band SAR (IW, ascending) with a 1 to 2 month revisit from 2014 to 2022 and derived statistics (Figure 2) and multitemporal maps of land subsidence as shown in Figure 3, where negative line-of-sight (LOS) values indicate subsidence and appear as orange to red on the maps, while positive values indicate stability or slight uplift. We found a persistent south-focused signal across the urban coastal tourism zone. Temporally, the series shows clear year-to-year pulses, with annual mean LOS values alternating between near-neutral and elevated positives that culminate in peaks in 2014 and 2018. Annual mean LOS values were near neutral in 2015 at -3.6 mm, in 2019 at -0.5 mm, and in 2022 at -0.5 mm, and they were higher and positive in 2014 at +22.2 mm with SD 9.1 mm, in 2016 at +4.7 mm with SD 10.1 mm, in 2017 at +15.5 mm with SD 8.8 mm, in 2018 at +35.4 mm with SD 8.5 mm, in 2020 at +7.7 mm with SD 6.6 mm, and in 2021 at +9.1 mm with SD 3.6 mm. Variability peaked in 2016 with SD 10.1

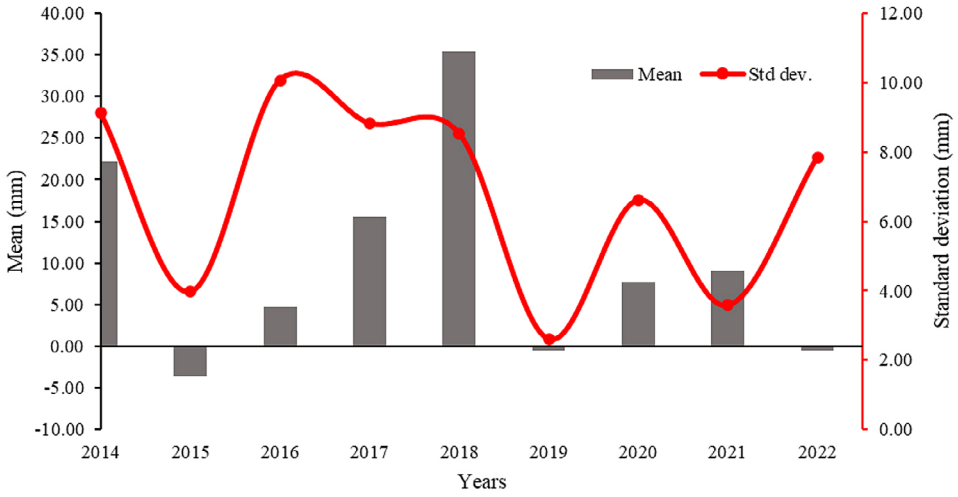

Figure 2. Annual land subsidence statistics (mean and standard deviation) for 2014 to 2022

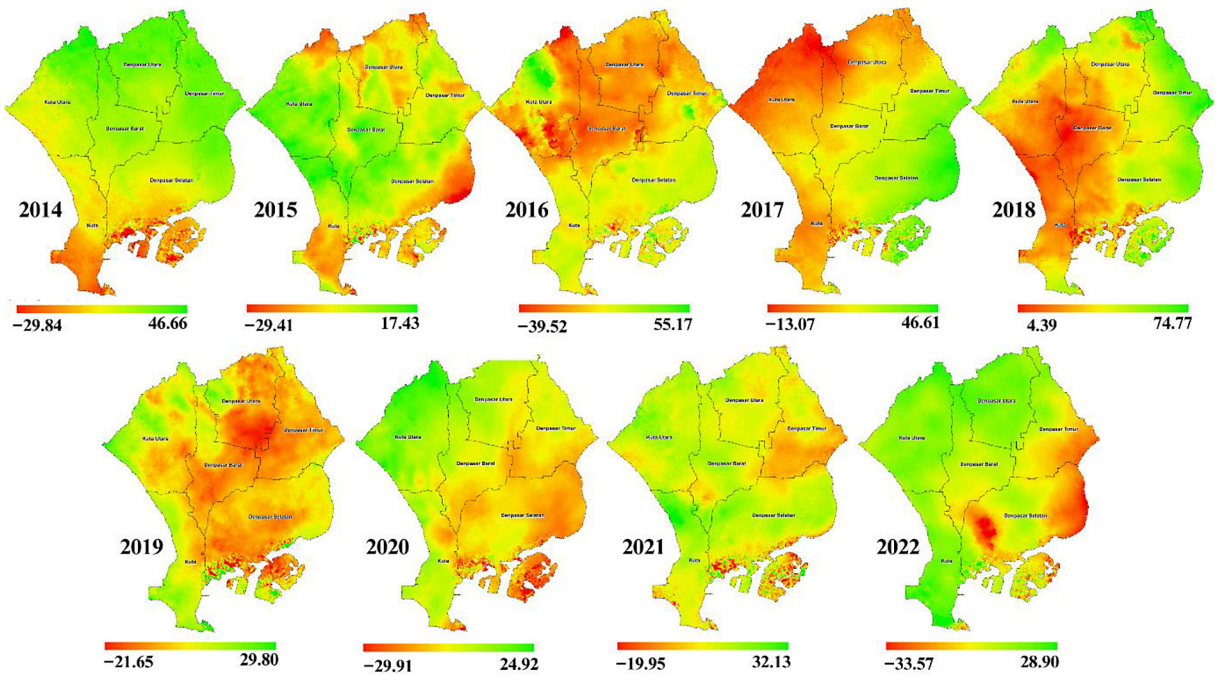

Figure 3. Spatiotemporal distribution of land subsidence (mm) across the coastal tourism zone of Bali, 2014 to 2022

mm despite the small mean, while 2019 to 2021 remained comparatively stable with low means from −0.5 to +9.1 mm and tight spreads of SD 2.6 to 3.6 mm. By 2022 the mean returned close to 0 mm while SD rose to 7.9 mm, indicating more heterogeneous behaviour within the zone.

Spatially, we observed consistent year-to-year shifts in subsidence hotspots across the southern urban tourism zone, with clusters migrating among Sanur, North Kuta, and the West and North Denpasar subdistricts. In 2014 subsidence extended across southern Denpasar and Kuta. In 2015 it concentrated in Sanur, South Denpasar. During 2016 to 2017 peaks moved to North Kuta and to West or North Denpasar, including Kerobokan Klod, Dalung, Dauh Puri, Padang Sambian, Padang Sambian Klod, and Padang Sambian Kaja. In 2018 the dominant area shifted west toward Padang Sambian Klod and Padang Sambian Kaja as well as Seminyak, Legian, and Kuta. In 2019 indications were widespread across built-up Denpasar with maxima near Dangin Puri. From 2020 to 2022 the pattern migrated toward the center to east, with recurring signals in Sanur at -1 to -29 mm and a notable 2022 pocket in Pemogan at -9 to -33 mm. On the maps, the orange to red tones consistently mark the strongest negative displacement.

Inter-annual changes corroborate these patterns. The largest subsidence rate occurred from 2018 to 2019 at -60 mm/yr, followed by -50 mm/yr in 2015, -40 mm/yr in 2017 and 2022, and -20 mm/yr in 2016 and 2021. Over nine years the worst-affected locations reached -70 mm/yr, while zone-wide averages peaked at -40 mm/yr during 2018 to 2019. These rates align with the mapped progression of hotspots from south and west toward the center and east, with repeated activity in Sanur and a distinct pocket in Pemogan in 2022 (Table 1).

Linking land subsidence and built-up density

We analyzed Sentinel-1 C-band InSAR (IW, ascending) for 2014–2022 and paired line-of-sight (LOS) displacement rasters with the built-up density layer to extract pixel values for statistical testing, and we selected 500 sampling points purposively from the mapped subsidence pattern and the distribution of dense urban fabric, which we also used as anchors for the 2022 field survey (Figure 4). In the field we documented wall cracking and localized road depressions that align with the mapped clusters, with the clearest on-site evidence in residential areas of South Denpasar and West Denpasar.

Across the coastal tourism zone, annual subsidence rates typically range from -10 to -60 mm/yr, with the most affected locations reaching about -70 mm/yr over 2014–2022, and the zone-wide mean over the period is approximately -40 mm/yr. The spatiotemporal maps show recurrent hotspots in West Denpasar (Dauh Puri and Padang Sambian), South Denpasar (Sanur and Pemogan), and North Kuta (Dalung). Although the footprint of maximum subsidence shifts by year, these districts repeatedly fall in the upper tail of the distribution, and the persistence observed on the maps is consistent with the 2022 ground observations of cracking and localized pavement settlement.

We quantified the relationship between subsidence and built-up density for each year from 2016 to 2022 using correlation and coefficient of determination calculated from the 500 pixel samples, and the full results are reported in Table 2. The coefficients of determination are very low, on the order of $R^2 = 0.0006$ to 0.012, and the corresponding correlation coefficients cluster near zero, spanning roughly $r = -0.11$ to $+0.008$. These figures indicate that, at the whole-area scale,

Table 1. Interannual land subsidence rate statistics (mm/yr), 2014–2024

Δ Years	Minimum	Mean	Max
Δ (2014–2015)	-46.00	-26.00	-11.00
Δ (2015–2016)	-17.00	10.00	45.00
Δ (2016–2017)	-40.00	12.00	30.00
Δ (2017–2018)	1.00	17.00	52.00
Δ (2018–2019)	-56.00	-36.00	-19.00
Δ (2019–2020)	-7.00	7.00	24.00
Δ (2020–2021)	-15.00	4.00	17.00
Δ (2021–2022)	-39.00	-16.00	4.00
Δ (2014–2022)	-65.00	-38.00	0.001

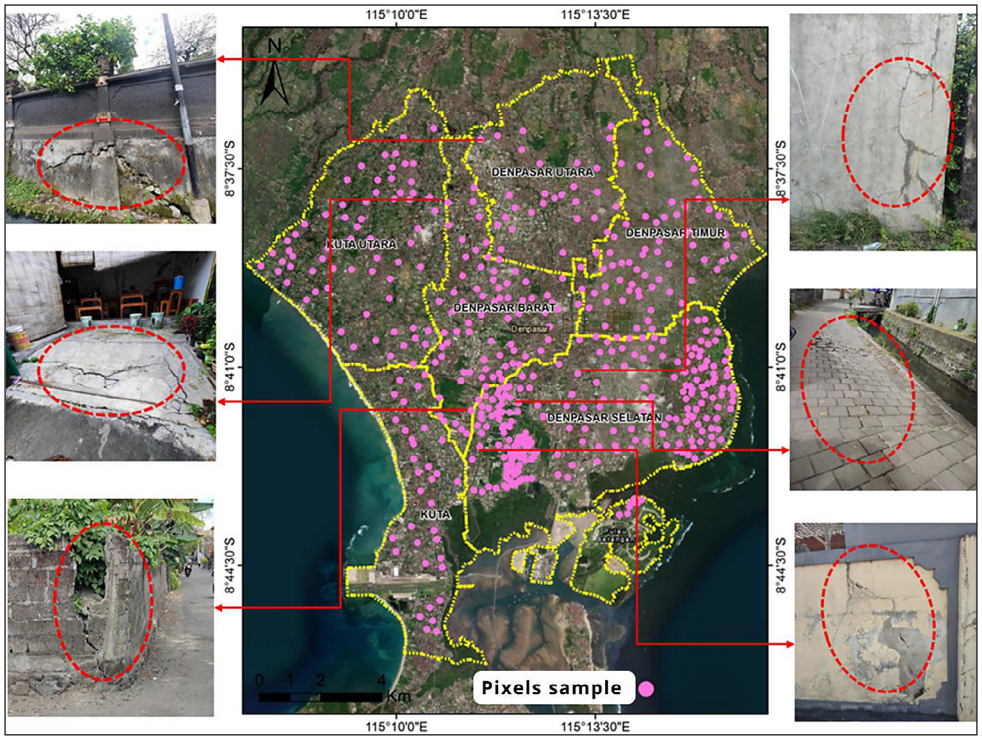

Figure 4. Sample locations for extracting pixel values (land subsidence and built-up land spectral index values), totaling 500 points. These sample locations are also used as ground checks for land subsidence events in residential areas

built-up density explains little of the variance in the InSAR-derived subsidence, which agrees with the mapped pattern where strong negative LOS values appear along parts of the coast as well as in selected inland neighborhoods rather than tracking density uniformly. Across the full tourism zone and Denpasar's urban core, subsidence and built-up density are only very weakly related. To probe this further, we re-estimated their correlation within zones exhibiting both high built-up density and relatively elevated annual subsidence rates (Figure 5), using (n ≈ 10,000 pixel samples) the outcome was consistent, indicating a very weak association. The correlation coefficient (r = 0.045) underscores this weakness, and the coefficient of determination (R^2 = 0.0021) shows that only ~0.21% of the variance in subsidence is explained by built-up density, with the remainder attributable to factors outside the model. Even so, the relationship is statistically significant: the coefficient p-value and the model's ANOVA Significance F are both $p = 5.1 \times 10^{-6}$ (< 0.05). Hence, while built-up density exerts a detectable effect, its contribution is minimal, implying that other drivers are likely more influential.

The time series reveals persistent subsidence concentrated in specific districts at rates typically between −10 and −60 mm/yr, with local extremes near −70 mm/yr. Field surveys corroborate these clusters, documenting wall cracking and minor

Table 2. The relationship between land subsidence and the built-up density

Data years	Coefficient determines (R^2)	Correlations (r)
2016	0.012	-0.11
2017	0.008	-0.09
2018	0.003	-0.06
2019	0.0006	-0.02
2020	0.004	0.006
2021	0.003	0.005
2022	0.007	0.008

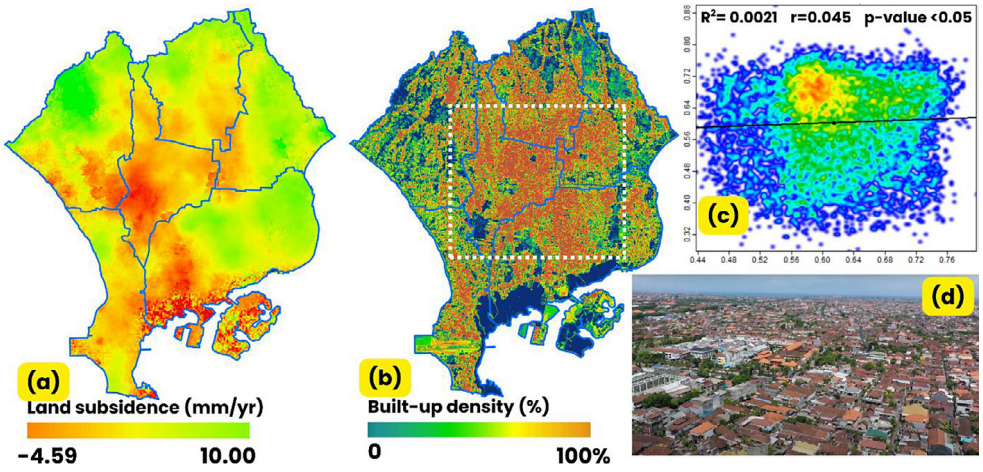

Figure 5. (a) Mean land subsidence, 2014 to 2022 (mm/yr); (b) mean built-up density, 2016 to 2022; the white line delineates the highest-density zone; (c) pixel-level linkage between built-up density and land subsidence; (d) field photograph illustrating conditions in a high-density

differential settlement in South and West Denpasar. Taken together, the mapped patterns, numerical summaries, and ground observations show that built-up density is not a strong predictor at the scale of the entire study area, but exhibits a weak, localized association within the highest-density strip. In the final section, we convey that the factors that have not been revealed are a challenge for us and future researchers to uncover what causes land subsidence in this tourism area and urban center.

DISCUSSIONS

Land deformation is a situation when the surface of the land changes horizontally and vertically (Ma et al., 2023). This is caused by many factors such as earthquakes, landslides, surface loads, groundwater extraction, and other geological disasters (Chen et al., 2023; Fan et al., 2019). Natural land subsidence occurs regionally, covering large areas, or locally, affecting only a small portion of the land surface. This is usually caused by the presence of cavities beneath the surface of the ground (Ma et al., 2023; Othman et al., 2018).

The process or movement of land subsidence has occurred in various regions around the world, especially in major cities (Sarah, 2022; Sukmawati et al., 2021; Zhang et al., 2019). The subsidence of the land surface that accumulates over a certain period can reach a decrease of several meters, causing damage to urban infrastructure, which may then disrupt the stability of the economy and social life in the area (Huning et al., 2024).

Land subsidence in North Denpasar and Kerobokan ranges from -8 mm to -19 mm/yr. Such conditions occur due to groundwater usage in the southern coastal areas (Dwiputra et al., 2020). Land subsidence has also occurred in West, South Denpasar, and Kuta (-100 mm to -200 mm). However, the exact factors influencing this are not yet known (Yastika et al., 2020). Our research complements both spatially and temporally and covers tourist areas that have not been studied by previous researchers, even though these tourist areas are important and urgent to explore. Our findings show that the rate of land subsidence is 27.14 mm/year, based on annual Sentinel 1-SAR data for the period 2014–2022. This information provides a basis for the management of urban areas and tourist regions in the future, to avoid the phenomenon of continuous land subsidence.

Another common phenomenon in this area due to land subsidence is the annual flooding that inundates urban areas and tourism industry centers (Diara et al., 2024; Suyarto et al., 2023; Trigunasih and Saifulloh, 2022). The increasing number of urban transportation, besides causing traffic congestion, also contributes to the greenhouse gas emissions that add to the land mass load. The spatial-temporal pattern of the land subsidence map is observed, with the phenomenon not only located in tourist centers but also following the main road routes. The information from this finding is important for future spatial planning, so that the expansion of built-up areas can be controlled and the tourism areas can be made safe and comfortable.

The coastal emphasis in our maps reflects known limits of C-band InSAR in mangrove and intertidal settings and should be read with caution. Over dense vegetation the radar senses the canopy rather than the ground, so wind, moisture and tidal effects lower coherence and destabilize phase unwrapping exactly along the shore. At 80 m pixel spacing many edge pixels mix land and water, and even with a water mask applied during unwrapping some near-shore pixels remain valid and can carry phase steps inland as narrow negative LOS bands. No external tropospheric correction was applied, so coastal humidity gradients and sea-breeze structure can imprint long-wavelength stripes that resemble gentle deformation. Values are referenced to a highest-coherence point and may retain small orbital or DEM ramps, and ascending-only geometry blends vertical motion with the east–west component. Together these factors create both random noise and systematic bias at the coast, including on Serangan Island and other mangrove margins, and they explain why some narrow shoreline belts appear as high subsidence.

These coastal artifacts also depress the area-wide relationship with the built environment. Many of the most negative LOS values occur in pixels dominated by vegetation or land–water mixtures rather than by built-up density, so they add variance that is unrelated to urban loading and they drag whole-area correlations toward zero. When the analysis is confined to coherent, fully urbanized pixels, mixed-pixel and canopy effects are largely excluded and the signal better reflects processes that plausibly scale with urban fabric, which is why the focused test in the highest-density strip yields a small positive correlation ($r = 0.045$; $R^2 = 0.21\%$) even though the region-wide association remains weak.

Uncertainty is therefore highest for single-year coastal pixels and lowest for multi-year, coherent urban clusters. Reported rates near mangroves and tidal flats should be treated as qualitative to semi-quantitative indicators rather than definitive vertical subsidence, and scene-wide means and pairwise deltas can shift by millimetres to centimetres under different referencing or residual ramps without changing the rank order of inland hotspots. The most reliable inferences come from patterns that persist across years on stable, high-coherence ground.

To reduce these limitations in follow-up work and to inform policy, researchers should prioritize stricter shoreline treatment (coherence masking and an inland buffer), explicit ramp removal with re-referencing to a demonstrably stable point, tide-stage aware pair selection, complementary descending tracks to separate vertical and horizontal components using look vectors, and time-series processing with atmospheric correction. Local government should interpret coastal belts as screening signals, not design values, and focus engineering investigation and monitoring on persistent inland hotspots while requiring settlement-aware design and groundwater management for new works in high-risk districts.

CONCLUSSIONS

Sentinel-1 DInSAR and field checks confirm persistent land subsidence across Bali's urban tourism corridor, concentrated in parts of South and West Denpasar and North Kuta. Citywide, the link with built-up density is very weak; using decade-average data and a focused test within the densest urban belt, the association remains weak, positive, and localized, indicating that urban form alone does not explain the regional pattern. Interpretation near mangrove and intertidal belts carries higher uncertainty due to vegetation motion, mixed land-water pixels at ~80 m, and unmodeled coastal atmosphere; nonetheless, the multi-year persistence of inland clusters and their field confirmation provide robust evidence of ongoing ground lowering in key neighbourhoods. We recommend treating these results as a screening baseline for risk-aware planning: prioritize geotechnical investigation and settlement-aware design in recurring hotspots; strengthen groundwater monitoring and management where pumping may contribute to subsidence; maintain an integrated InSAR-GNSS-leveling monitoring program; and incorporate subsidence risk into zoning and permits for new coastal and high-load developments. Further analysis should jointly consider built-up density with geology, soils, hydrology, and groundwater levels to refine attribution and support targeted mitigation.

Acknowledgments

We thank the anonymous reviewers for their constructive comments that improved this manuscript. This work was supported by DIPA PNBP Universitas Udayana, Fiscal Year 2025, under the Research Implementation Assignment Agreement Letter No. B/229.195/UN14.4.A/PT.01.03/2025, dated April 28, 2025.

REFERENCES

1. Abidin, H. Z., Andreas, H., Gumilar, I., Fukuda, Y., Pohan, Y. E., Deguchi, T. (2011). Land subsidence of Jakarta (Indonesia) and its relation with urban development. *Natural Hazards*, *59*(3). https://doi.org/10.1007/s11069-011-9866-9
2. Abidin, H. Z., Andreas, H., Gumilar, I., Sidiq, T. P., Fukuda, Y. (2013). Land subsidence in coastal city of Semarang (Indonesia): Characteristics, impacts and causes. *Geomatics, Natural Hazards and Risk*, *4*(3). https://doi.org/10.1080/19475705.2012.692336
3. Andyana, I. W. S., As-Syakur, A. R., Sunarta, I. N., Suyarto, R., Diara, I. W., Susila, K. D., Saifulloh, M., Kusmiyarti, T. B., Wiyanti, W. (2023). Urban tourism expansion monitoring by remote sensing and random forest. *IOP Conference Series: Earth and Environmental Science*, *1180*(1). https://doi.org/10.1088/1755-1315/1180/1/012046
4. Bai, Z., Wang, Y., Balz, T. (2022). Beijing Land Subsidence Revealed Using PS-InSAR with Long Time Series TerraSAR-X SAR Data. *Remote Sensing*, *14*(11). https://doi.org/10.3390/rs14112529
5. Bhayunagiri, I. B. P., Saifulloh, M. (2023). Urban footprint extraction derived from worldview-2 satellite imagery by random forest and k-nearest neighbours algorithm. *IOP Conference Series: Earth and Environmental Science*, *1200*(1), 12043.
6. Chen, W., Zhong, C., Qin, X., Wang, L. (2023). Geological Disaster: An overview. *Intelligent Interpretation for Geological Disasters: From Space-Air-Ground Integration Perspective*, 1–23.
7. Cian, F., Blasco, J. M. D., Carrera, L. (2019). Sentinel-1 for monitoring land subsidence of coastal cities in Africa using PSInSAR: A methodology based on the integration of SNAP and staMPS. *Geosciences (Switzerland)*, *9*(3). https://doi.org/10.3390/geosciences9030124
8. Darbaghshahi, F. N., Mohammadi, M. R., Soryani, M. (2022). Cloud removal in remote sensing images using generative adversarial networks and SAR-to-optical image translation. *IEEE Transactions on Geoscience and Remote Sensing*, *60*. https://doi.org/10.1109/TGRS.2021.3131035
9. Diara, I. W., Susila, K. D., Wiyanti, W., Sunarta, I. N., Kusmiyarti, T. B., Saifulloh, M. (2024). Exploring the influence of various land use land cover on land surface temperature of coastal tourism areas in Bali using Landsat 9. *Environmental Research, Engineering and Management*, *80*(2), 118–132.
10. Dwiputra, M. R., Osawa, T., Karang, I. W. G. A. (2020). Land subsidence analysis observed by ps-insar method in southern part of Bali, Indonesia (a case study of denpasar and badung area). *ACRS 2020 - 41st Asian Conference on Remote Sensing*. https://doi.org/10.24843/ejes.2020.v14.i02.p11
11. Fajrin, F., Almegi, A., Bakari, A., Ramadhan, R., Antomi, Y. (2021). Enviromental monitoring of land subsidence in the coastal area of Padang city using Sentinel 1 Sar Dataset. *Sumatra Journal of Disaster, Geography and Geography Education*, *5*(1). https://doi.org/10.24036/sjdgge.v5i1.359
12. Fan, X., Scaringi, G., Korup, O., West, A. J., van Westen, C. J., Tanyas, H., Hovius, N., Hales, T. C., Jibson, R. W., Allstadt, K. E., Zhang, L., Evans, S. G., Xu, C., Li, G., Pei, X., Xu, Q., Huang, R. (2019). Earthquake-induced chains of geologic hazards: patterns, mechanisms, and impacts. In *Reviews of Geophysics* 57(2). https://doi.org/10.1029/2018RG000626
13. Fernández-Torres, E. A., Cabral-Cano, E., Solano-Rojas, D., Salazar-Tlaczani, L., Gárcia-Venegas, J., Marquez-Azúa, B., Graham, S., Villarnobo-Gonzalez, K. M. (2024). Country-scale assessment of urban areas, population, and households exposed to land subsidence using Sentinel-1 InSAR, and GPS time series. *Natural Hazards*, *120*(2). https://doi.org/10.1007/s11069-023-06259-5
14. Gorelick, N., Hancher, M., Dixon, M., Ilyushchenko, S., Thau, D., Moore, R. (2017). Google Earth Engine: Planetary-scale geospatial analysis for everyone. *Remote Sensing of Environment*, *202*. https://doi.org/10.1016/j.rse.2017.06.031
15. Hakim, W. L., Achmad, A. R., Lee, C. W. (2020). Land subsidence susceptibility mapping in jakarta using functional and meta-ensemble machine learning algorithm based on time-series insar data. *Remote Sensing*, *12*(21). https://doi.org/10.3390/rs12213627
16. Harintaka, H., Suhadha, A. G., Syetiawan, A., Ardha, M., Rarasati, A. (2024). Current land subsidence in Jakarta: a multi-track SBAS InSAR analysis during 2017–2022 using C-band SAR data. *Geocarto International*, *39*(1), 2364726.
17. Huning, L. S., Love, C. A., Anjileli, H., Vahedifard, F., Zhao, Y., Chaffe, P. L. B., Cooper, K., Alborzi, A., Pleitez, E., Martinez, A. (2024). Global land subsidence: Impact of climate extremes and human activities. *Reviews of Geophysics*, *62*(4), e2023RG000817.
18. Hussain, M. A., Chen, Z., Shoaib, M., Shah, S. U., Khan, J., Ying, Z. (2022). Sentinel-1A for monitoring land subsidence of coastal city of Pakistan using Persistent Scatterers In-SAR technique. *Scientific Reports*, *12*(1). https://doi.org/10.1038/s41598-022-09359-7
19. Ibrahim, H. B., Salah, M., Zarzoura, F., El-Mewafi, M. (2024). Differential synthetic aperture radar (SAR) interferometry for detection land subsidence in Derna City, Libya. *Journal of Applied Geodesy*, *18*(3). https://doi.org/10.1515/jag-2023-0087
20. Karimzadeh, S., Matsuoka, M. (2020). Remote sensing x-band sar data for land subsidence and pavement monitoring. *Sensors (Switzerland)*, *20*(17). https://doi.org/10.3390/s20174751

21. Ma, S., Qiu, H., Zhu, Y., Yang, D., Tang, B., Wang, D., Wang, L., Cao, M. (2023). Topographic changes, surface deformation and movement process before, during and after a rotational landslide. *Remote Sensing*, *15*(3). https://doi.org/10.3390/rs15030662
22. Othman, A., Sultan, M., Becker, R., Alsefry, S., Alharbi, T., Gebremichael, E., Alharbi, H., Abdelmohsen, K. (2018). Use of geophysical and remote sensing data for assessment of aquifer depletion and related land deformation. In *Surveys in Geophysics* 39(3). https://doi.org/10.1007/s10712-017-9458-7
23. Pawluszek-Filipiak, K., Borkowski, A. (2020). Integration of DInSAR and SBAS techniques to determine mining-related deformations using Sentinel-1 data: The case study of rydultowy mine in Poland. *Remote Sensing*, *12*(2). https://doi.org/10.3390/rs12020242
24. Rafiei, F., Gharechelou, S., Golian, S., Johnson, B. A. (2022). Aquifer and land subsidence interaction assessment using Sentinel-1 data and DInSAR technique. *ISPRS International Journal of Geo-Information*, *11*(9). https://doi.org/10.3390/ijgi11090495
25. Rateb, A., Abotalib, A. Z. (2020). Inferencing the land subsidence in the Nile Delta using Sentinel-1 satellites and GPS between 2015 and 2019. *Science of the Total Environment*, *729*. https://doi.org/10.1016/j.scitotenv.2020.138868
26. Sahu, S. R., Rawat, K. S. (2023). Analysis of Land subsidencein coastal and urban areas by using various techniques– Literature review. In *Indonesian Journal of Geography* 55(3). https://doi.org/10.22146/ijg.83675
27. Sarah, D. (2022). Land subsidence hazard in Indonesia: Present research and challenges ahead. *Riset Geologi Dan Pertambangan*, *32*(2). https://doi.org/10.14203/risetgeotam2022.v32.1195
28. Sarah, D., Soebowo, E., Satriyo, N. A. (2021). Review of the land subsidence hazard in pekalongan delta, central java: Insights from the subsurface. *Rudarsko Geolosko Naftni Zbornik*, *36*(4). https://doi.org/10.17794/rgn.2021.4.13
29. Sowter, A., Bin Che Amat, M., Cigna, F., Marsh, S., Athab, A., Alshammari, L. (2016). Mexico City land subsidence in 2014–2015 with Sentinel-1 IW TOPS: Results using the Intermittent SBAS (ISBAS) technique. *International Journal of Applied Earth Observation and Geoinformation*, *52*. https://doi.org/10.1016/j.jag.2016.06.015
30. Sudarma, I., Saifulloh, M., Diara, I. W., As-Syakur, A. (2024). Carbon stocks dynamics of urban green space ecosystems using time-series vegetation indices. *Ecological Engineering & Environmental Technology*, *25*(9).
31. Sukmawati, R., Waqar, M. M., Syafriani, Yohandri, Sumantyo, J. T. S. (2021). Land subsidence estimation using DinSAR method ALOS PALSAR image in Padang City West Sumatra, Indonesia. *Pillar of Physics*, *14*(1). https://doi.org/10.24036/10673171074
32. Sunarta, I. N., Saifulloh, M. (2022a). Coastal tourism: impact for built-up area growth and correlation to vegetation and water indices derived from Sentinel-2 remote sensing imagery. *Geojournal of Tourism and Geosites, 41*(2). https://doi.org/10.30892/gtg.41223-857
33. Sunarta, I. N., Saifulloh, M. (2022b). Spatial variation of NO_2 levels during the covid-19 pandemic in the bali tourism area. *Geographia Technica*, *17*(1). https://doi.org/10.21163/GT_2022.171.11
34. Sunarta, I. N., Suyarto, R., Saifulloh, M., Wiyanti, W., Susila, K. D., Kusumadewi, L. G. L. (2022). Surface urban heat island (SUHI) phenomenon in bali and lombok tourism areas based on remote sensing. *Journal of Southwest Jiaotong University*, *57*(4). https://doi.org/10.35741/issn.0258-2724.57.4.44
35. Suyarto, R., Wiyanti, Saifulloh, M., Fatahillah, A. W., Diara, I. W., Susila, K. D., Kusmiyarti, T. B. (2023). Hydrological approach for flood overflow estimation in Buleleng Watershed, Bali. *International Journal of Safety and Security Engineering*, *13*(5). https://doi.org/10.18280/ijsse.130512
36. Trigunasih, N. M., Saifulloh, M. (2022). The Investigating water infiltration conditions caused by annual urban flooding using integrated remote sensing and geographic information systems. *Journal of Environmental Management & Tourism*, *13*(5), 1467–1480.
37. Wang, L., Xu, X., Yu, Y., Yang, R., Gui, R., Xu, Z., Pu, F. (2019). SAR-to-optical image translation using supervised cycle-consistent adversarial networks. *IEEE Access*, *7*. https://doi.org/10.1109/ACCESS.2019.2939649
38. Yastika, P. E., Shimizu, N., Pujianiki, N. N., Temaja, I. G. R. M., Antara, I. N. G., Osawa, T. (2020). Detection of silent subsidence over extensive area by SBAS DInSAR: A case study of Southern Bali, Indonesia. *E3S Web of Conferences*, *153*. https://doi.org/10.1051/e3sconf/202015302003
39. Zha, Y., Gao, J., Ni, S. (2003). Use of normalized difference built-up index in automatically mapping urban areas from TM imagery. *International Journal of Remote Sensing*, *24*(3). https://doi.org/10.1080/01431160304987
40. Zhang, Y., Liu, Y., Jin, M., Jing, Y., Liu, Y., Liu, Y., Sun, W., Wei, J., Chen, Y. (2019). Monitoring land subsidence in wuhan city (China) using the SBAS-INSAR method with radarsat-2 imagery data. *Sensors (Switzerland)*, *19*(3). https://doi.org/10.3390/s19030743